1 # Assessing contributions of natural surface and anthropogenic emissions to
2 atmospheric mercury in a fast developing region of Eastern China from
3 2015 to 2018

4 Xiaofei Qin[1], Leiming Zhang[2], Guochen Wang[1], Xiaohao Wang[3], Qingyan Fu[3], Jian Xu[1], Hao Li[1],

5 Jia Chen[1], Qianbiao Zhao[3], Yanfen Lin[3], Juntao Huo[3], Fengwen Wang[4], Kan Huang[1,5,6,*], Congrui

6 Deng[1,*]

7

8 [1] Center for Atmospheric Chemistry Study, Shanghai Key Laboratory of Atmospheric Particle
9   Pollution and Prevention (LAP3), Department of Environmental Science and Engineering, Fudan
10   University, Shanghai, 200433, China
11 [2] Air Quality Research Division, Science and Technology Branch, Environment and Climate Change
12   Canada, Toronto, M3H 5T4, Canada
13 [3] Shanghai Environmental Monitoring Center, Shanghai, 200030, China
14 [4] State Key Laboratory of Coal Mine Disaster Dynamics and Control, College of Environment and
15   Ecology, Chongqing University, Chongqing 400030, China
16 [5] Institute of Eco-Chongming (IEC), Shanghai, 202162, China
17 [6] Institute of Atmospheric Sciences, Fudan University, Shanghai 200433, China

18

19 **Abstract**

20 Mercury (Hg) is a global toxic pollutant that can be released into the atmosphere through

21 anthropogenic and natural sources. The uncertainties in the estimated emission amounts are much

22 larger from natural than anthropogenic sources. A method was developed in the present study to

23 quantify the contributions of natural surface mercury emissions to ambient gaseous elemental

24 mercury (GEM) concentrations through application of positive matrix factorization (PMF) analysis

25 with temperature, O_3, and NH_3 as indicators of GEM emissions from natural surfaces. GEM

26 concentrations were continuously monitored at a 2-hourly resolution at a regional background site

27 in the Yangtze River Delta in Eastern China during 2015-2018. Annual average GEM concentrations

28 were in the range of 2.03-3.01 ng/m^3, with a strong decreasing trend at a rate of -0.32±0.07 ng m^{-3}

29 yr^{-1} from 2015 to 2018, which was mostly caused by reduced anthropogenic emissions since 2013.

30 The estimated contributions from natural surface emissions of mercury to the ambient GEM

31 concentrations were in the range of 0.90-1.01 ng/m^3 on annual average with insignificant interannual

32 changes, but the relative contribution increased significantly from 36% in 2015 to 53% in 2018,

33 gradually surpassing those from anthropogenic sources.

34

35 **1. Introduction**

36   Mercury has long been recognized as a toxic pollutant due to its bioaccumulation and health

37   effects (Driscoll et al., 2013b;Clarkson and Magos, 2006;Schroeder and Munthe, 1998;Horowitz et

38   al., 2017;Fu et al., 2012;Wright et al., 2018). Mercury in the atmosphere can be transported globally,

39   mostly in the form of gaseous elemental mercury (GEM) due to its long lifetime in air (Driscoll et

40   al., 2013a). Clarifying sources and quantifying emissions from the major sources of atmospheric

41   mercury are critical for understanding the biogeochemical cycle of mercury and developing mercury

42   reduction strategies. Mercury in the atmosphere is released from both natural and anthropogenic

43   sources. Natural sources include volcanoes. geological weathering, forest fires, re-emissions of pre-

44   deposited mercury from natural surfaces, etc (Gustin et al., 2008;Mason and Sheu, 2002). Among

45   these sources, emissions from natural surfaces are the major ones and a number of studies have been

46   devoted to understanding the processes of natural surface emissions (Xu et al., 1999;Lindberg et al.,

47   2002;Kocman et al., 2013). Anthropogenic sources mainly include coal-fired power plants, non-

48   ferrous smelters, and waste incineration (Friedli et al., 2009). Globally, natural sources released

49   about 5200 tons mercury into the atmosphere on an annual basis, which contributed up to two-thirds

50   of the global atmospheric mercury budget, while those by anthropogenic sources was estimated to

51   be around 2300 tons (Pirrone et al., 2010). In China, the total mercury emissions released from

52   natural and anthropogenic sources were estimated to be 574.5 ton yr^{-1}, and 571 ton yr^{-1}, respectively

53   (Wang et al., 2016;Zhang et al., 2015).

54   During the past decades, anthropogenic emissions of mercury in Europe and North America

55   have been reduced significantly through phasing out mercury from many commercial products as

56   well as benefiting from SO_2 and NO_x emission reduction from coal-fired utilities, resulting in

57   considerable decrease in atmospheric mercury concentrations in these regions (e.g., approximately

58   1-2% yr^{-1} decrease from 1990 to 2013) (Streets et al., 2011;Zhang et al., 2016). In China,

59   anthropogenic mercury emissions decreased from 571 ton in 2013 to 444 ton in 2017 due to the co-

60   benefits of aggressive air pollutant control measures implemented in this period (Liu et al., 2019a).

61   GEM concentrations measured at a rural site north of Shanghai showed a substantially decreasing

62   trend from 2014 to 2016 (Tang et al., 2018).

63   With the decrease of anthropogenic mercury emissions in many parts of the world (Zhang et

64   al., 2016), the contributions of natural emissions to total mercury budget are expected to be more

65   important. However, the trends of natural emissions are still unclear due to the difficulties in directly

Atmospheric
Chemistry
and Physics
Discussions

66 measuring GEM emissions from natural surfaces (Zhu et al., 2015). Existing estimates of GEM

67 emission from natural sources have large uncertainties (e.g., from 1500 to 5207 Mg yr^{-1} on global

68 scale), limiting our understanding of the role of natural emissions in the global mercury cycle (Song

69 et al., 2015;Wang et al., 2014b). For example, a study at rural Beijing showed that modeled GEM

70 concentrations were underestimated by about 40% than measurements from April to September

71 2009 due to the absence of natural emission inventories (Wang et al., 2014a). Hence, it is meaningful

72 to develop a method to quantify the contributions of natural surface emissions to total mercury

73 budget in the atmosphere, especially in China where anthropogenic emissions have been fast

74 decreasing in recent years.

75   The purpose of the present study is to differentiate the contributions of natural surface

76 emissions and anthropogenic emissions to the measured ambient GEM concentrations collected

77 during a four-year period at a regional background site in the Yangtze River Delta (YRD) of Eastern

78 China. This was done by conducting positive matrix factorization (PMF) analysis with identified

79 variables as tracers of natural surface mercury emissions. Results presented in this study provide an

80 approach that can be potentially used for improving mercury emission databases for natural sources.

81

82 **2. Materials and methods**

83 **2.1 Site description**

84   Shanghai, situated in the YRD region, is one of the most developed cities in China. Like in

85 many other cities in China, severe air pollutions have occurred frequently in this city in the past

86 decades. A supersite has been set up next to the Dianshan Lake in Qingpu District of rural Shanghai

87 (Figure 1) as part of the framework of State Environmental Protection Scientific Observation and

88 Research Station. This supersite is designed to represent the regional scale air pollution

89 characteristics in the YRD region based on the following two considerations: (1) it is located in the

90 conjunction area of Shanghai, Jiangsu, and Zhejiang provinces; and (2) there are no large point

91 sources such as coal-fired power plants, nonferrous metal smelting, and cement production within

92 20km distance surrounding the site. This site was established in 2013 and its capacity has been

93 gradually built by measuring a set of atmospheric parameters, including meteorological factors,

94 trace gases, aerosol physical and chemical parameters, vertical profiles of ozone and particles, etc.

95 More detailed descriptions of the site can be found elsewhere (Qin et al., 2019;Duan et al., 2017).

96

2.2 Measurements of gaseous elemental mercury

An automated mercury vapor analyzer Tekran 2537B/1130/1135 was installed on the third floor of a building for real time continuous GEM measurements since January 2015. GEM was measured based on the principle of cold vapor atomic fluorescence spectroscopy (CVAFS) (Landis and Keeler, 2002). Briefly, ambient GEM was collected on gold traps and then thermally decomposed to GEM before detection. The sampling interval of GEM was 5 minutes with a flow rate of 1L/min. More details of this instrument can be found elsewhere (Mao et al., 2008).

Strict quality control procedures were followed during the sampling process. Denuders and quartz filters were prepared and cleaned according to the instructions in Tekran technical notes before sampling. Routine calibration with internal permeation source was performed every 47 hours and manual injections of standard saturated mercury vapor were conducted to ensure the accuracy of these automated calibrations. The KCl-coated denuder, Teflon-coated glass inlet, and impactor plate were replaced weekly and quartz filters were replaced monthly. Individual extremely high GEM concentrations that occasionally happened were regarded as outliers and were excluded from the data analysis.

112

2.3 Measurements of other air pollutants and meteorological parameters

Water soluble ions in $PM_{2.5}$ and soluble gases were continuously measured by Monitor for Aerosols and Gases in ambient Air (MARGA) operated at a flow rate of 16.7 L/min with a time resolution of one hour, as detailed in (Chang et al., 2016). Briefly, water-soluble gases in the airflow were removed by an absorbing liquid, then the particles were induced by a supersaturation of water vapor to grow into droplets before they were collected and transported into the analytical chamber.

Trace metals in $PM_{2.5}$ were continuously measured by using the Xact 625 ambient metals monitor (Cooper Environmental, Beaverton, OR, USA) operated at a flow rate of 16.7 L/min with hourly resolution, as detailed in (Yu et al., 2019). Briefly, the particles in the airflow were deposited onto a Teflon filter tape, and then transported into the spectrometer where the particles were analyzed with an X-ray fluorescence.

Ozone, carbon monoxide, and $PM_{2.5}$ were measured by Thermo Fisher 49i, Thermo Fisher 48i-TLE, and Thermo Fisher 1405-F, respectively. Meteorological parameters including ambient

126   temperature, wind speed, and wind direction were obtained at the sampling site by using the

127   automatic weather station (AWS). Bivariate polar plots (BPP) were applied in this study to explore

128   how GEM concentrations change with different wind direction and wind speed, which has proven

129   to be a reliable method for identifying different source regions (Carslaw et al., 2006;Carslaw and

130   Ropkins, 2012;Chang et al., 2017). Here, the open-source software "openair" in R was used to create

131   BPPs (Carslaw and Ropkins, 2012).

132

133   **2.4 Positive matrix factorization (PMF)**

134   The PMF model has been proven to be a useful tool to provide quantitative source profiles and

135   source contributions (Xu et al., 2017;Gibson et al., 2015). The basic principle of PMF is that

136   concentrations of the samples were determined by the source profiles with different contributions,

137   which can be descried as follows:

138    $$X_{ij} = \sum_{k=1}^{P} g_{ik} f_{kj} + e_{ij} \quad (1)$$

139   where X_{ij} represents the concentration of the jth species in the ith sample, g_{ik} is the contribution

140   of the kth factor in the ith sample, f_{kj} provides the information of the mass fraction of the jth

141   species in the kth factor, e_{ij} is the residual for specific measurement, and P represents the number

142   of factors.

143   The objective function expressed in Eq. (2) below, which is the sum of the square of the

144   difference between the measured and modeled concentrations weighted by the concentration

145   uncertainties, needs to be minimized before the PMF model determines the optimal non-negative

146   factor profiles and contributions.(Cheng et al., 2015)

147    $$Q = \sum_{i=1}^{n} \sum_{j=1}^{m} \left(\frac{X_{ij} - \sum_{k=1}^{p} A_{ik} F_{kj}}{S_{ij}} \right)^2 (2)$$

148   where X_{ij} represents the concentration of the jth contamination in the ith sample, m is the total

149   number of pollutant, and n is the total number of sample. A_{ik} represents the contribution of the kth

150   factor on the ith sample and F_{kj} represents the mass fraction of the jth pollutant in the kth factor.

151   S_{ij} is the uncertainty of the jth pollutant on the ith factor and P is the number of factors. In this

152   study, we explored the number of factors from three to eight with the optimal solutions determined

153   by the slope of the Q value versus the number of factors. For each run, the stability and reliability

154   of the outputs were assessed by referring to the Q value, residual analysis, and correlation

155   coefficients between observed and predicted concentrations. Finally, we found that a six-factor

156   solution showed the most stable results and gave the most reasonable interpretation. A dataset

157   containing uncertainty values of each species was created and digested into the model, with the error

158   fraction being assumed to be 15% for GEM concentration and 10% for other compounds (Xu et al.,

159   2017;Polissar et al., 1998).

160   It should be noted that Fpeak model run at the strength of 0.5 was done by using the rotation

161   tools in PMF and the results were summarized in Table S1. For all seasons, the increase of the Q-

162   value due to the Fpeak rotation with a dQ was less than 1% of the Base Run Q (robust) value.

163   According to the User Guide of PMF5.0, it was acceptable when the %dQ was less than 5%. The

164   profiles and contributions of each source were examined and there were no significant differences

165   between the factor contributions of Base Run and rotation results. Hence, the Base Run results were

166   used in this study.

167

168   **2.5 Annual changes of anthropogenic mercury emission in China and YRD**

169   It was reported that the annual anthropogenic atmospheric mercury emission in China

170   significantly increased from 147 tons in 1978 to 549 tons in 2010 (Wu et al., 2016). In more recent

171   years, in order to cope with the severe air pollution situation, the Chinese government has taken

172   many rigorous and ambitious measures such as introduction of ultra-low emissions standards on

173   power plants and phasing out of small factories with high-emissions (Zheng et al., 2018). As a result,

174   mercury emissions from anthropogenic sources have since been declining in China. For the five-

175   year period of 2013-2017, annual total anthropogenic mercury emissions in China were estimated

176   to be 571, 547, 528, 486, and 444 tons, respectively, or a total decline of 127 tons. During the same

177   period, the reduction of anthropogenic mercury emissions reached 60 tons in eastern China (Liu et

178   al., 2019a).

179

180   **3. Results and Discussion**

181   **3.1 The measured gaseous elemental mercury**

182   **3.1.1 Decreasing trend of gaseous elemental mercury**

183   The measured annual mean GEM concentrations were 3.01 ± 1.03, 2.58 ± 0.84, 2.52 ± 0.84,

184   and 2.03 ± 0.69 ng/m^3 from 2015 to 2018. By using the Theil-Sen function, monthly GEM exhibited

185   a significantly decreasing trend from 2015 to 2018 ($p<0.05$) with a rate of -0.32 ± 0.07 ng m^{-3} yr^{-1}

186   (Figure 2a). This decreasing trend was consistent with the trends of mass concentrations of $PM_{2.5}$

187   and SO_2 (Figure 2b & 2c), which were attributed to the implementation of the Clean Air Action

188   since 2013 in China (Zheng et al., 2018). As mentioned earlier (Section 2.5), the nationwide

189   reduction of anthropogenic mercury emissions should be largely responsible for the significant

190   decrease in GEM concentration observed at the YRD regional background site.

191   Seasonal average GEM concentrations decreased from 3.62 ng/m^3 to 2.17 ng/m^3 with a rate of

192   -0.37 ng m^{-3} yr^{-1} in spring, from 2.89 ng/m^3 to 1.98 ng/m^3 with a rate of -0.26 ng m^{-3} yr^{-1} in summer,

193   from 2.62 ng/m^3 to 1.94 ng/m^3 with a rate of -0.22 ng m^{-3} yr^{-1} in autumn, and from 2.91 ng/m^3 to

194   1.82 ng/m^3 with a rate of -0.35 ng m^{-3} yr^{-1} in winter (Figure 3). The decreasing rates of GEM were

195   ~30% lower in the warm seasons than the cold seasons. Considering that seasonal variations of

196   anthropogenic emission are minimum, the different seasonal decreasing rates of GEM should be

197   mostly caused by the seasonal-dependent emission amounts from natural sources, knowing that

198   natural emissions are controlled by solar radiation and temperature, among other factors (Howard

199   and Edwards, 2018;Pannu et al., 2014;Mason, 2009).

200

3.1.2 Impact of temperature on ambient gaseous elemental mercury

202   In a previous study we showed that GEM concentrations tended to rise with increasing

203   temperature in the YRD region, which was considered to be the effect of temperature-dependent

204   emission amounts from natural surfaces (Qin et al., 2019). Here, to qualitatively investigate the role

205   of natural surface emissions on ambient GEM concentration, diurnal profiles of the bi-hourly GEM

206   concentration and temperature are exhibited in Figure 4. If looking at the whole year data together,

207   moderate to high correlations were seen between the diurnal variations of GEM and temperature in

208   2016, 2017, and 2018 with R^2 being 0.30 to 0.86, except in 2015 with little correlation with R^2 being

209   only 0.03 (Figure 4a-4d). The maximum GEM concentrations generally appeared around 10AM -

210   14PM, mostly coincided with daily peak temperature. These findings provided strong evidence of

211   temperature-dependent GEM sources.

212   Due to the large differences in ambient temperature between warm (from June to November)

213   and cold (from December to May) seasons in the YRD region, the effects of temperature-dependent

214   GEM sources on the ambient GEM concentrations should be different in different seasons. As

215   expected, high correlations between GEM concentration and temperature were found in the warm

216   seasons with R^2 being in the range of 0.15 to 0.87 (Figures 4e-4h), while nearly no correlations in

217   the cold seasons (Figures 4i-4l). Thus, the influence of natural surface emissions on ambient GEM

218   concentration was important in the warm seasons, but may not be the case in the cold seasons. The

219   seasonal bivariate polar plots of GEM showed that high GEM concentrations were associated

220   frequently with air flows from the south and southwest and occasionally with those from the north,

221   particularly in summer (Figure S1). This was consistent with the findings in previous studies which

222   showed stronger natural surface emissions in South and Southwest China than North China (Wang

223   et al., 2016;Feng et al., 2005;Wang et al., 2006;Sommar et al., 2016). Hence, in the context of

224   significant reduction of anthropogenic mercury emission in China, especially in North China (Liu

225   et al., 2019b), natural surface emissions significantly impacted the ambient GEM concentrations at

226   this sampling site.

227

228   **3.2 Quantify the contributions from natural surface emissions to ambient gaseous elemental**

229   **mercury**

230   **3.2.1 Development of the approach**

231   A method is developed below for quantifying the contributions of GEM emissions from natural

232   surfaces to ambient GEM concentrations through application of the PMF model by introducing

233   specific variables related to natural surface emissions as traces. The first step is to identify what

234   variables are directly or indirectly related to the natural surface emissions of GEM. Temperature is

235   certainly a dominant one as has been demonstrated in existing soil-air fluxes studies of mercury

236   (Wang et al., 2014b;Zhu et al., 2016;Poissant and Casimir, 1998). The formation pathways of Hg^0

237   in soil are all related to temperature, an empirical rule suggests that a 10°C temperature increase

238   doubles the rates for chemical reaction near room temperature, which has been proven to be

239   applicable to Hg^{II} reduction in boreal soil (Moore and Carpi, 2005;Quinones and Anthony,

240   2011;Wang et al., 2016;Pannu et al., 2014). Discussions in Section 3.1.2 also suggested temperature

241   as a potentially useful tracer for predicting natural surface emissions of GEM. A second candidate

242   of tracers could be ambient NH_3 concentration because soil emissions of GEM and NH_3, both of

243   which are temperature-dependent, are treated in a similar way in air-quality modeling studies

244   (Wright and Zhang, 2015;Zhang et al., 2010). The third potential tracer could be O_3 concentration

245   because high temperature can promote the formation of O_3 (Kerr et al., 2019;Kerr and Waugh,

246   2018;Schnell and Prather, 2017). As shown in Figure S2, the mean diurnal variations of GEM

247   concentration highly correlated with ambient temperature as well as NH_3 and O_3 concentrations.

248   From this perspective, NH_3 and O_3 can be regarded as indirect proxies for the natural surface

249   emissions of GEM. In a previous study we have applied principal component analysis for source

250   apportionment of mercury in this area, and the source factor with high loadings for temperature,

251   NH_3, and O_3 was interpreted as natural surface emissions of GEM (Qin et al., 2019).

252   Hence, in this study, we included the data of temperature, NH_3, and O_3 into the PMF model to

253   apportion the sources of GEM. As shown in Figures S3-S18, the source apportionment results for

254   all the seasons of 2015-2018 all resolved a similar factor with high loadings of temperature and O_3

255   and moderate loadings of NH_3 and GEM. This factor was thought to be the natural surface emission

256   sources of mercury. As for the other resolved factors, the factor with high loadings of V and Ni

257   evidently represented shipping emissions. The factor with high loadings of Ca was assigned to

258   cement production. Moderate loadings of multiple species including Cr, Mn, and Fe was found in

259   one factor which were identified as iron and steel production. The factor with high loadings of NO

260   was identified as vehicle emissions. And the last factor was identified as coal combustion due to the

261   high loadings of As and Se, and moderate contributions of Pb and SO_4^{2-}.

262   In order to verify the PMF modeling results, we first examined the PMF model performance.

263   Table S2 shows the coefficient of determination (R^2) for GEM according to the observation-

264   prediction scatter plots (Figure S20-S23). The R^2 values ranged from 0.37 to 0.89, suggesting an

265   acceptable model performance. Figure S24-S27 display the time series of observed and predicted

266   GEM concentrations from 2015-2018, which revealed that, except for a few extremely high

267   observation values, the model can relatively well reproduce the observed GEM concentration on an

268   hourly basis. To further verify the reliability of the resolved factors, the correlations between the

269   mass contributions of all factors to GEM and temperature were examined on the basis of diurnal

270   profiles. As shown in Figure S19, positive correlation was only found between the natural surface

271   emission factor and temperature while the other resolved factors (i.e. vehicle emission, coal

272   combustion, shipping activities, cement production, and iron and steel production) did not show this

273   relationship. This further corroborated that by using temperature, NH_3, and O_3 as tracers, the natural

274   surface emissions of GEM can be identified and quantified.

275

276 **3.2.2 Increasing contributions from natural surface emissions to ambient gaseous elemental**

277 **mercury**

278   Figure 5 summarizes the contributions of natural surface emissions and anthropogenic

279 emissions to GEM on seasonal basis from 2015 – 2018. The contributions of natural surface

280 emissions to GEM were ~40% higher in summer (1.09 ± 0.58 ng/m^3) than winter (0.78 ± 0.54 ng/m^3).

281 Besides, the contributions of natural surface emissions to GEM exhibited an upward trend, e.g.,

282 increased from 32% to 52% in spring, 39% to 63% in summer, 41% to 53% in autumn, and 32% to

283 43% in winter, from 2015-2018 (Figure 5). In contrast, the contributions from anthropogenic sources

284 to GEM showed a downward trend, of which the decreased contribution from coal combustion

285 accounted the most. Coal combustion has been widely regarded as the dominant anthropogenic

286 source of mercury emissions at the global scale, and China is known as the largest coal producer

287 and consumer in the world (Zhang et al., 2012;Wu et al., 2006). Since 2013, a series of key air

288 pollution control measures have been applied in China to reduce the emission of air pollutants

289 (Zheng et al., 2018). YRD regions also took actions by regulating on the amount of coal

290 consumption, promoting renewable energy development and so on (Zheng et al., 2016). Hence, the

291 decreased contribution of coal combustion was attributed to the implementation of aggressive air

292 pollutant control measures in China in recent years, which subsequently led to an increase in the

293 relative contribution of natural surface emissions to GEM.

294   The absolute GEM concentrations contributed by both natural surface emissions and

295 anthropogenic emissions can be extracted from the PMF modeling results. Figure 6 exhibits the

296 monthly and yearly profiles from 2015 to 2018. Strong seasonal cycles of GEM contributed by

297 natural surface emissions were seen, corresponding to the seasonal pattern of ambient temperature

298 (Figure 6g) and the simulated monthly Hg fluxes from natural surface emissions in China (Wang et

299 al., 2016). The annual GEM concentration contributed by natural surface emissions was estimated

300 to be 0.94 ± 0.57 ng/m^3, 1.01 ± 0.63 ng/m^3, 1.00 ± 0.62 ng/m^3, and 0.90 ± 0.48 ng/m^3 from 2015 to

301 2018, respectively (Figure 6a & 6b), which almost remained unchanged. This could be mainly

302 explained by the little variation of annual temperature (Fig. 6h) and wind pattern from 2015 to 2018

303 (Fig. S28). On the contrary, the annual GEM concentration contributed by anthropogenic emissions

304 was estimated to be 1.67 ± 1.06 ng/m^3, 1.51 ± 0.77 ng/m^3, 1.38 ± 1.02 ng/m^3, and 0.80 ± 0.63 ng/m^3

305 from 2015 to 2018, respectively, showing an obvious decreasing trend (Figure 6c & 6d). It was

306   noted that the GEM concentration contributed by anthropogenic emissions dropped the most from

307   2017 to 2018 with a rate of around 40%. By referring to the Table S3, SO_2 and CO also decreased

308   significantly of about 35% and 18%. As SO_2 and CO were the main primary gaseous pollutants

309   emitted from fuel combustions, their sharp decreases indicated the significant reduction of

310   anthropogenic emissions which was probably responsible for large drop of GEM from 2017 to 2018.

311   Overall, the relative contribution of natural surface emissions to ambient GEM was on the rise, e.g.,

312   from 36% in 2015 to 53% in 2018 on annual average (Figures 6e & 6f).

313

314   **4. Conclusions and Implications**

315   Through a four-year continuous measurement of GEM in the suburbs of Shanghai, a clear

316   decreasing trend was observed with the rate of -0.32±0.07 ng m^{-3} yr^{-1}, which was mainly due to the

317   reduction of anthropogenic mercury emissions. The lower decreasing rate in warm seasons than in

318   cold seasons and the high correlation between GEM concentrations and temperature suggested that

319   natural surface emissions significantly impacted the GEM concentrations. By demonstrating that

320   temperature, O_3, and NH_3 can well serve as tracers of natural surface mercury emissions,

321   distinguishing natural vs. anthropogenic contributions to GEM was doable by introducing these

322   tracers into the PMF model. The results indicated that the contribution from anthropogenic mercury

323   emissions was declining, especially from coal combustion. The annual absolute contributions of

324   natural surface emissions were in the range of 0.90-1.01 ng/m^3, and the relative contribution of

325   natural surface emissions to GEM increasing form 36% in 2015 to 53% in 2018.

326   Measurements of GEM and other pollutants in a regional background area in Eastern China

327   demonstrated the effectiveness of emission control policies in this and surrounding regions in China

328   in recent years. The decreasing contributions from anthropogenic sources and the relatively stable

329   contributions from natural surface emissions to the ambient GEM have resulted in the relative

330   contributions of natural surface emissions surpassing those of anthropogenic emissions in more

331   recent years. This trend will likely continue for some years considering the current pollution levels

332   in China which needs further pollution abatement. This implies that even though the anthropogenic

333   emissions of mercury would continue to decrease, the legacy mercury in the natural surfaces will

334   continue to emit steadily for a long period of time. In addition, the natural release of mercury could

335   be enhanced under climate warming scenario. Hence, the atmospheric mercury concentration in

336 YRD or other parts of China will remain at relatively high levels in the near future, which brings

337 big challenges to China's policies on mercury emissions reduction. The methodology developed in

338 the present study could also shed some light on source apportionment of atmospheric mercury in

339 the other regions of the world, and has potential for improving emission databases from natural

340 surfaces where ambient GEM and auxiliary data are available.

341

342 **Acknowledgments**

346

347 **Author contribution**

348 X.Q. and K. H. designed this study. X.Q. performed measurements and data analysis. X.W., Q.F.,

349 Q.Z., Y.L., and J.H. performed data collection. X.Q., L.Z., K.H., and C.D. wrote the paper. All have

350 commented and reviewed the paper.

351

352 **Competing interests**

353 The authors declare that they have no conflict of interest.

354

355 **Data availability**

356 All data used in this study can be requested from K.H. (huangkan@fudan.edu.cn).

357

358 **References:**

359 Carslaw, D., Beevers, S., Ropkins, K., and Bell, M.: Detecting and quantifying aircraft and other on-
360 airport contributions to ambient nitrogen oxides in the vicinity of a large international airport,
361 Atmospheric Environment, 40, 5424-5434, 10.1016/j.atmosenv.2006.04.062, 2006.
362 Carslaw, D. C., and Ropkins, K.: openair — An R package for air quality data analysis, Environmental
363 Modelling & Software, 27-28, 52-61, 10.1016/j.envsoft.2011.09.008, 2012.
364 Chang, Y., Zou, Z., Deng, C., Huang, K., Collett, J. L., Lin, J., and Zhuang, G.: The importance of vehicle
365 emissions as a source of atmospheric ammonia in the megacity of Shanghai, Atmospheric Chemistry and
366 Physics, 16, 3577-3594, 10.5194/acp-16-3577-2016, 2016.
367 Chang, Y., Deng, C., Cao, F., Cao, C., Zou, Z., Liu, S., Lee, X., Li, J., Zhang, G., and Zhang, Y.:
368 Assessment of carbonaceous aerosols in Shanghai, China - Part 1: long-term evolution, seasonal

369 variations, and meteorological effects, Atmospheric Chemistry and Physics, 17, 9945-9964, 10.5194/acp-
370 17-9945-2017, 2017.

371 Cheng, I., Xu, X., and Zhang, L.: Overview of receptor-based source apportionment studies for speciated
372 atmospheric mercury, Atmos. Chem. Phys., 15, 7877-7895, 10.5194/acp-15-7877-2015, 2015.

373 Clarkson, T. W., and Magos, L.: The toxicology of mercury and its chemical compounds, Crit. Rev.
374 Toxicol., 36, 609-662, 10.1080/10408440600845619, 2006.

375 Driscoll, C. T., Mason, R. P., Chan, H. M., Jacob, D. J., and Pirrone, N.: Mercury as a global pollutant:
376 sources, pathways, and effects, Environmental science & technology, 47, 4967-4983, 10.1021/es305071v,
377 2013a.

378 Driscoll, C. T., Mason, R. P., Chan, H. M., Jacob, D. J., and Pirrone, N.: Mercury as a Global Pollutant:
379 Sources, Pathways, and Effects, Environmental science & technology, 47, 4967-4983, 2013b.

380 Duan, L., Wang, X., Wang, D., Duan, Y., Cheng, N., and Xiu, G.: Atmospheric mercury speciation in
381 Shanghai, China, Sci. Total Environ., 578, 460-468, https://doi.org/10.1016/j.scitotenv.2016.10.209,
382 2017.

383 Feng, X. B., Wang, S. F., Qiu, G. A., Hou, Y. M., and Tang, S. L.: Total gaseous mercury emissions from
384 soil in Guiyang, Guizhou, China, J. Geophys. Res.-Atmos., 110, 2005.

385 Friedli, H. R., Arellano, A. F., Cinnirella, S., and Pirrone, N.: Initial Estimates of Mercury Emissions to
386 the Atmosphere from Global Biomass Burning, Environmental science & technology, 43, 3507-3513,
387 10.1021/es802703g, 2009.

388 Fu, X. W., Feng, X. B., Sommar, J., and Wang, S. F.: A review of studies on atmospheric mercury in
389 China, Sci. Total Environ., 421, 73-81, 10.1016/j.scitotenv.2011.09.089, 2012.

390 Gibson, M. D., Haelssig, J., Pierce, J. R., Parrington, M., Franklin, J. E., Hopper, J. T., Li, Z., and Ward,
391 T. J.: A comparison of four receptor models used to quantify the boreal wildfire smoke contribution to
392 surface PM2.5 in Halifax, Nova Scotia during the BORTAS-B experiment, Atmospheric Chemistry and
393 Physics, 15, 815-827, 10.5194/acp-15-815-2015, 2015.

394 Gustin, M. S., Lindberg, S. E., and Weisberg, P. J.: An update on the natural sources and sinks of
395 atmospheric mercury, Appl. Geochem., 23, 482-493, 10.1016/j.apgeochem.2007.12.010, 2008.

396 Horowitz, H. M., Jacob, D. J., Zhang, Y., Dibble, T. S., Slemr, F., Amos, H. M., Schmidt, J. A., Corbitt,
397 E. S., Marais, E. A., and Sunderland, E. M.: A new mechanism for atmospheric mercury redox chemistry:
398 implications for the global mercury budget, Atmospheric Chemistry and Physics, 17, 6353-6371,
399 10.5194/acp-17-6353-2017, 2017.

400 Howard, D., and Edwards, G. C.: Mercury fluxes over an Australian alpine grassland and observation of
401 nocturnal atmospheric mercury depletion events, Atmospheric Chemistry and Physics, 18, 129-142, 2018.

402 Kerr, G. H., and Waugh, D. W.: Connections between summer air pollution and stagnation,
403 Environmental Research Letters, 13, 10.1088/1748-9326/aad2e2, 2018.

404 Kerr, G. H., Waugh, D. W., Strode, S. A., Steenrod, S. D., Oman, L. D., and Strahan, S. E.: Disentangling
405 the Drivers of the Summertime Ozone-Temperature Relationship Over the United States, 124, 10503-
406 10524, 10.1029/2019jd030572, 2019.

407 Kocman, D., Horvat, M., Pirrone, N., and Cinnirella, S.: Contribution of contaminated sites to the global
408 mercury budget, Environmental Research, 125, 160-170, 10.1016/j.envres.2012.12.011, 2013.

409 Landis, M. S., and Keeler, G. J.: Atmospheric mercury deposition to Lake Michigan during the Lake
410 Michigan Mass Balance Study, Environmental science & technology, 36, 4518-4524, 10.1021/es011217b,
411 2002.

412 Lindberg, S. E., Zhang, H., Vette, A. F., Gustin, M. S., Barnett, M. O., and Kuiken, T.: Dynamic flux

413   chamber measurement of gaseous mercury emission fluxes over soils: Part 2 - effect of flushing flow rate

414   and verification of a two-resistance exchange interface simulation model, Atmospheric Environment, 36,

415   847-859, 10.1016/s1352-2310(01)00502-7, 2002.

416   Liu, K., Wu, Q., Wang, L., Wang, S., Liu, T., Ding, D., Tang, Y., Li, G., Tian, H., Duan, L., Wang, X., Fu,

417   X., Feng, X., and Hao, J.: Measure-Specific Effectiveness of Air Pollution Control on China's

418   Atmospheric Mercury Concentration and Deposition during 2013-2017, Environmental science &

419   technology, 10.1021/acs.est.9b02428, 2019a.

420   Liu, K., Wu, Q., Wang, L., Wang, S., Liu, T., Ding, D., Tang, Y., Li, G., Tian, H., Duan, L., Wang, X., Fu,

421   X., Feng, X., and Hao, J.: Measure-Specific Effectiveness of Air Pollution Control on China's

422   Atmospheric Mercury Concentration and Deposition during 2013-2017, Environmental science &

423   technology, 53, 8938-8946, 10.1021/acs.est.9b02428, 2019b.

424   Mao, H., Talbot, R. W., Sigler, J. M., Sive, B. C., and Hegarty, J. D.: Seasonal and diurnal variations of

425   Hg degrees over New England, Atmospheric Chemistry and Physics, 8, 1403-1421, 10.5194/acp-8-1403-

426   2008, 2008.

427   Mason, R. P., and Sheu, G. R.: Role of the ocean in the global mercury cycle, Global Biogeochemical

428   Cycles, 16, 40-41-40-14, 10.1029/2001gb001440, 2002.

429   Mason, R. P.: Mercury Emissions from Natural Processes and their Importance in the Global Mercury

430   Cycle, Mercury Fate and Transport in the Global Atmosphere: Emissions, Measurements and Models,

431   edited by: Pirrone, N., and Mason, R., 173-191 pp., 2009.

432   Moore, C., and Carpi, A.: Mechanisms of the emission of mercury from soil: Role of UV radiation, J.

433   Geophys. Res.-Atmos., 110, 10.1029/2004jd005567, 2005.

434   Pannu, R., Siciliano, S. D., and O'Driscoll, N. J.: Quantifying the effects of soil temperature, moisture

435   and sterilization on elemental mercury formation in boreal soils, Environmental Pollution, 193, 138-146,

436   10.1016/j.envpol.2014.06.023, 2014.

437   Pirrone, N., Cinnirella, S., Feng, X., Finkelman, R. B., Friedli, H. R., Leaner, J., Mason, R., Mukherjee,

438   A. B., Stracher, G. B., Streets, D. G., and Telmer, K.: Global mercury emissions to the atmosphere from

439   anthropogenic and natural sources, Atmos. Chem. Phys., 10, 5951-5964, 10.5194/acp-10-5951-2010,

440   2010.

441   Poissant, L., and Casimir, A.: Water-air and soil-air exchange rate of total gaseous mercury measured at

442   background sites, Atmospheric Environment, 32, 883-893, 10.1016/s1352-2310(97)00132-5, 1998.

443   Polissar, A. V., Hopke, P. K., and Paatero, P.: Atmospheric aerosol over Alaska - 2. Elemental composition

444   and sources, J. Geophys. Res.-Atmos., 103, 19045-19057, 10.1029/98jd01212, 1998.

445   Qin, X., Wang, X., Shi, Y., Yu, G., Zhao, N., Lin, Y., Fu, Q., Wang, D., Xie, Z., Deng, C., and Huang, K.:

446   Characteristics of atmospheric mercury in a suburban area of east China: sources, formation mechanisms,

447   and regional transport, Atmos. Chem. Phys., 19, 5923-5940, 10.5194/acp-19-5923-2019, 2019.

448   Quinones, J. L., and Anthony, C. J. J. o. E. Q.: An Investigation of the Kinetic Processes Influencing

449   Mercury Emissions from Sand and Soil Samples of Varying Thickness, 40, 647-, 2011.

450   Schnell, J. L., and Prather, M. J.: Co-occurrence of extremes in surface ozone, particulate matter, and

451   temperature over eastern North America, 114, 2854-2859, 10.1073/pnas.1614453114 %J Proceedings of

452   the National Academy of Sciences, 2017.

453   Schroeder, W. H., and Munthe, J.: Atmospheric mercury - An overview, Atmospheric Environment, 32,

454   809-822, 10.1016/s1352-2310(97)00293-8, 1998.

455   Sommar, J., Zhu, W., Shang, L., Lin, C.-J., and Feng, X.: Seasonal variations in metallic mercury (Hg-0)

456   vapor exchange over biannual wheat-corn rotation cropland in the North China Plain, Biogeosciences,

457   13, 2029-2049, 10.5194/bg-13-2029-2016, 2016.

458   Song, S., Selin, N. E., Soerensen, A. L., Angot, H., Artz, R., Brooks, S., Brunke, E. G., Conley, G.,

459   Dommergue, A., Ebinghaus, R., Holsen, T. M., Jaffe, D. A., Kang, S., Kelley, P., Luke, W. T., Magand,

460   O., Marumoto, K., Pfaffhuber, K. A., Ren, X., Sheu, G. R., Slemr, F., Warneke, T., Weigelt, A., Weiss-

461   Penzias, P., Wip, D. C., and Zhang, Q.: Top-down constraints on atmospheric mercury emissions and

462   implications for global biogeochemical cycling, Atmospheric Chemistry and Physics, 15, 7103-7125,

463   10.5194/acp-15-7103-2015, 2015.

464   Streets, D. G., Devane, M. K., Lu, Z. F., Bond, T. C., Sunderland, E. M., and Jacob, D. J.: All-Time

465   Releases of Mercury to the Atmosphere from Human Activities, Environmental science & technology,

466   45, 10485-10491, 10.1021/es202765m, 2011.

467   Tang, Y., Wang, S. X., Wu, Q. R., Liu, K. Y., Wang, L., Li, S., Gao, W., Zhang, L., Zheng, H. T., Li, Z.

468   J., and Hao, J. M.: Recent decrease trend of atmospheric mercury concentrations in East China: the

469   influence of anthropogenic emissions, Atmospheric Chemistry and Physics, 18, 8279-8291, 10.5194/acp-

470   18-8279-2018, 2018.

471   Wang, D. Y., He, L., Shi, X. J., Wei, S. Q., and Feng, X. B.: Release flux of mercury from different

472   environmental   surfaces   in   Chongqing,   China,   Chemosphere,   64,   1845-1854,

473   10.1016/j.chemosphere.2006.01.054, 2006.

474   Wang, L., Wang, S. X., Zhang, L., Wang, Y. X., Zhang, Y. X., Nielsen, C., McElroy, M. B., and Hao, J.

475   M.: Source apportionment of atmospheric mercury pollution in China using the GEOS-Chem model,

476   Environmental Pollution, 190, 166-175, 10.1016/j.envpol.2014.03.011, 2014a.

477   Wang, X., Lin, C. J., and Feng, X.: Sensitivity analysis of an updated bidirectional air-surface exchange

478   model for elemental mercury vapor, Atmospheric Chemistry and Physics, 14, 6273-6287, 10.5194/acp-

479   14-6273-2014, 2014b.

480   Wang, X., Lin, C.-J., Yuan, W., Sommar, J., Zhu, W., and Feng, X.: Emission-dominated gas exchange

481   of elemental mercury vapor over natural

482   surfaces in China, Atmospheric Chemistry and Physics, 16, 11125-11143, 10.5194/acp-16-11125-2016,

483   2016.

484   Wright, L. P., and Zhang, L. M.: An approach estimating bidirectional air-surface exchange for gaseous

485   elemental mercury at AMNet sites, Journal of Advances in Modeling Earth Systems, 7, 35-49,

486   10.1002/2014ms000367, 2015.

487   Wright, L. P., Zhang, L., Cheng, I., Aherne, J., and Wentworth, G. R.: Impacts and Effects Indicators of

488   Atmospheric Deposition of Major Pollutants to Various Ecosystems - A Review, Aerosol Air Qual. Res.,

489   18, 1953-1992, 10.4209/aaqr.2018.03.0107, 2018.

490   Wu, Q. R., Wang, S. X., Li, G. L., Liang, S., Lin, C. J., Wang, Y. F., Cai, S. Y., Liu, K. Y., and Hao, J. M.:

491   Temporal Trend and Spatial Distribution of Speciated Atmospheric Mercury Emissions in China During

492   1978-2014, Environmental science & technology, 50, 13428-13435, 10.1021/acs.est.6b04308, 2016.

493   Wu, Y., Wang, S. X., Streets, D. G., Hao, J. M., Chan, M., and Jiang, J. K.: Trends in anthropogenic

494   mercury emissions in China from 1995 to 2003, Environmental science & technology, 40, 5312-5318,

495   10.1021/es060406x, 2006.

496   Xu, X., Liao, Y., Cheng, I., and Zhang, L.: Potential sources and processes affecting speciated

497   atmospheric mercury at Kejimkujik National Park, Canada: comparison of receptor models and data

498   treatment methods, Atmospheric Chemistry and Physics, 17, 1381-1400, 10.5194/acp-17-1381-2017,

499   2017.

500   Xu, X. H., Yang, X. S., Miller, D. R., Helble, J. J., and Carley, R. J.: Formulation of bi-directional

501   atmosphere-surface exchanges of elemental mercury, Atmospheric Environment, 33, 4345-4355,
502   10.1016/s1352-2310(99)00245-9, 1999.

503   Yu, Y., He, S., Wu, X., Zhang, C., Yao, Y., Liao, H., Wang, Q., and Xie, M.: PM2.5 elements at an urban
504   site in Yangtze River Delta, China: High time-resolved measurement and the application in source
505   apportionment, Environ Pollut, 253, 1089-1099, 10.1016/j.envpol.2019.07.096, 2019.

506   Zhang, L., Wright, L. P., and Asman, W. A. H.: Bi-directional air-surface exchange of atmospheric
507   ammonia: A review of measurements and a development of a big-leaf model for applications in regional-
508   scale air-quality models, J. Geophys. Res.-Atmos., 115, 10.1029/2009jd013589, 2010.

509   Zhang, L., Wang, S. X., Meng, Y., and Hao, J. M.: Influence of Mercury and Chlorine Content of Coal
510   on Mercury Emissions from Coal-Fired Power Plants in China, Environmental science & technology, 46,
511   6385-6392, 10.1021/es300286n, 2012.

512   Zhang, L., Wang, S., Wang, L., Wu, Y., Duan, L., Wu, Q., Wang, F., Yang, M., Yang, H., Hao, J., and Liu,
513   X.: Updated emission inventories for speciated atmospheric mercury from anthropogenic sources in
514   China, Environmental science & technology, 49, 3185-3194, 10.1021/es504840m, 2015.

515   Zhang, Y., Jacob, D. J., Horowitz, H. M., Chen, L., Amos, H. M., Krabbenhoft, D. P., Slemr, F., St Louis,
516   V. L., and Sunderland, E. M.: Observed decrease in atmospheric mercury explained by global decline in
517   anthropogenic emissions, Proc Natl Acad Sci U S A, 113, 526-531, 10.1073/pnas.1516312113, 2016.

518   Zheng, B., Tong, D., Li, M., Liu, F., Hong, C., Geng, G., Li, H., Li, X., Peng, L., Qi, J., Yan, L., Zhang,
519   Y., Zhao, H., Zheng, Y., He, K., and Zhang, Q.: Trends in China's anthropogenic emissions since 2010 as
520   the consequence of clean air actions, Atmospheric Chemistry and Physics, 18, 14095-14111,
521   10.5194/acp-18-14095-2018, 2018.

522   Zheng, J., Jiang, P., Qiao, W., Zhu, Y., and Kennedy, E.: Analysis of air pollution reduction and climate
523   change mitigation in the industry sector of Yangtze River Delta in China, Journal of Cleaner Production,
524   114, 314-322, 10.1016/j.jclepro.2015.07.011, 2016.

525   Zhu, W., Sommar, J., Lin, C. J., and Feng, X.: Mercury vapor air-surface exchange measured by
526   collocated micrometeorological and enclosure methods - Part II: Bias and uncertainty analysis,
527   Atmospheric Chemistry and Physics, 15, 5359-5376, 10.5194/acp-15-5359-2015, 2015.

528   Zhu, W., Lin, C.-J., Wang, X., Sommar, J., Fu, X., and Feng, X.: Global observations and modeling of
529   atmosphere–surface exchange of elemental mercury: a critical review, Atmospheric Chemistry and
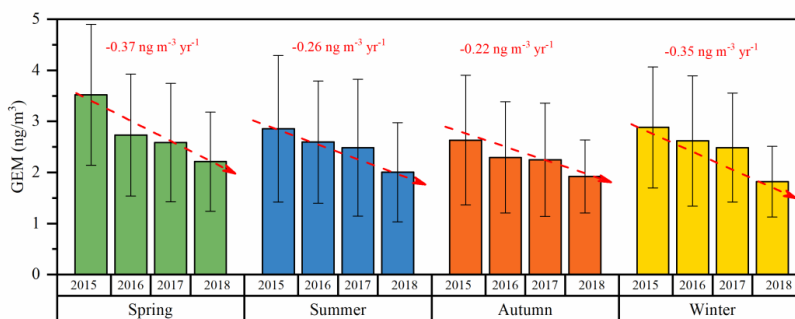530   Physics, 16, 4451-4480, 10.5194/acp-16-4451-2016, 2016.

531
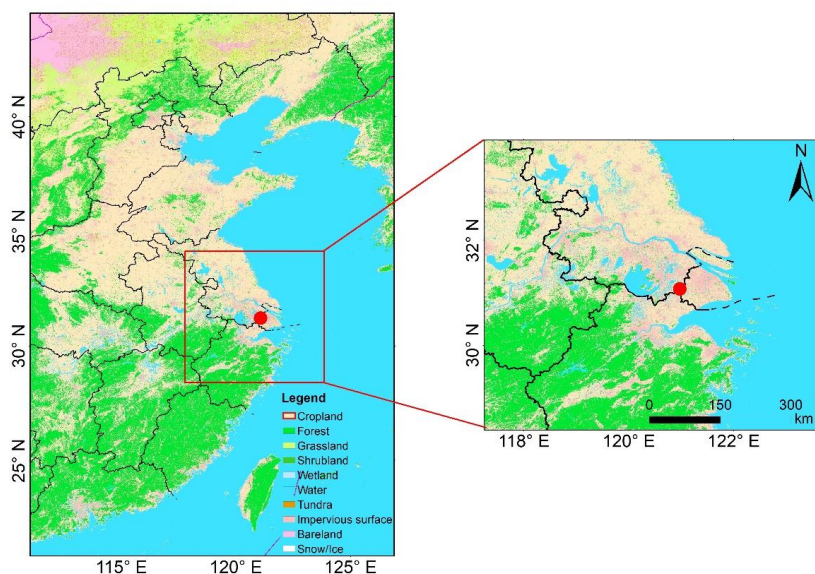
Figure 1. The location of the Dianshan Lake (DSL) site in Shanghai, China. Different colors in the map represent different land cover types.
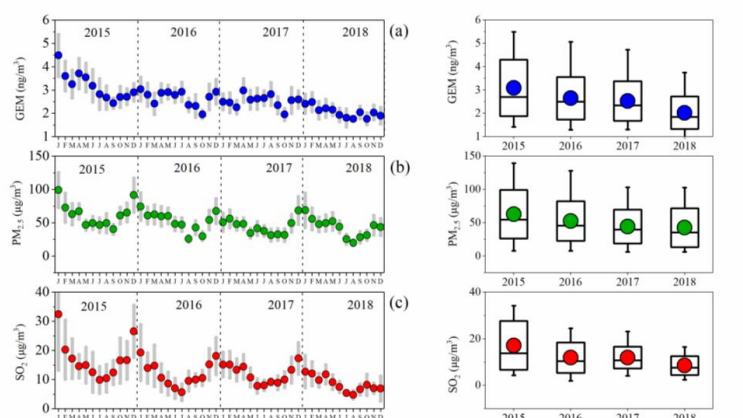
Figure 2. Monthly and annual variations of (a) GEM, (b) $PM_{2.5}$, and (c) SO_2 concentrations from 2015 to 2018.
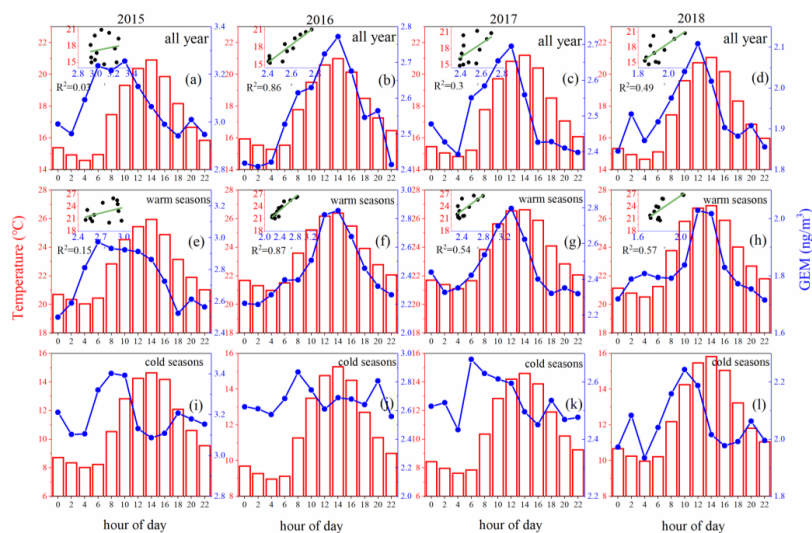
539

540   Figure 3. Seasonal variations of GEM concentrations from 2015 to 2018. The variation rates of

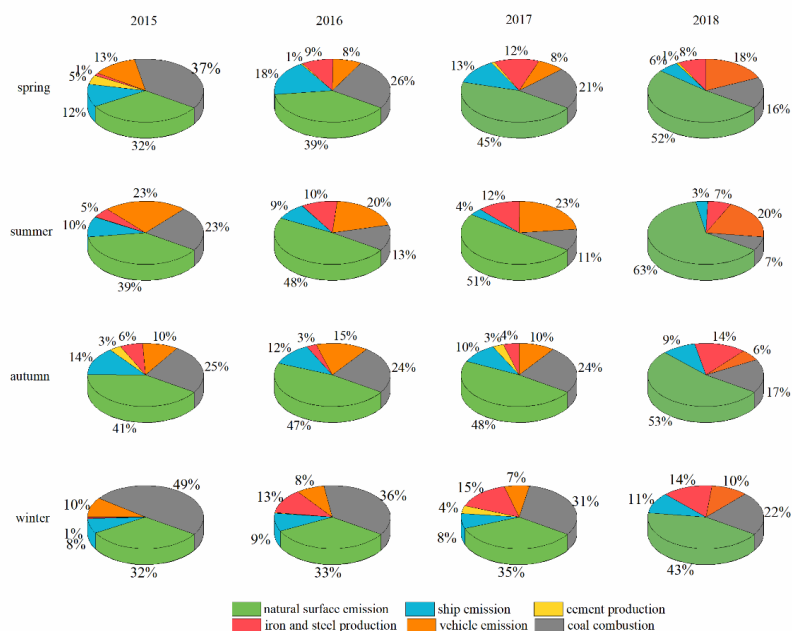541   GEM for each season are also shown in the figure.

542

543

544   Figure 4. Diurnal patterns of bi-hourly GEM concentrations and temperature for the whole year (a-

545   d), warm seasons (e-h), and cold seasons (i-l) during 2015 – 2018, respectively. The linear

546   correlations between GEM and temperature are inserted as inner figures.
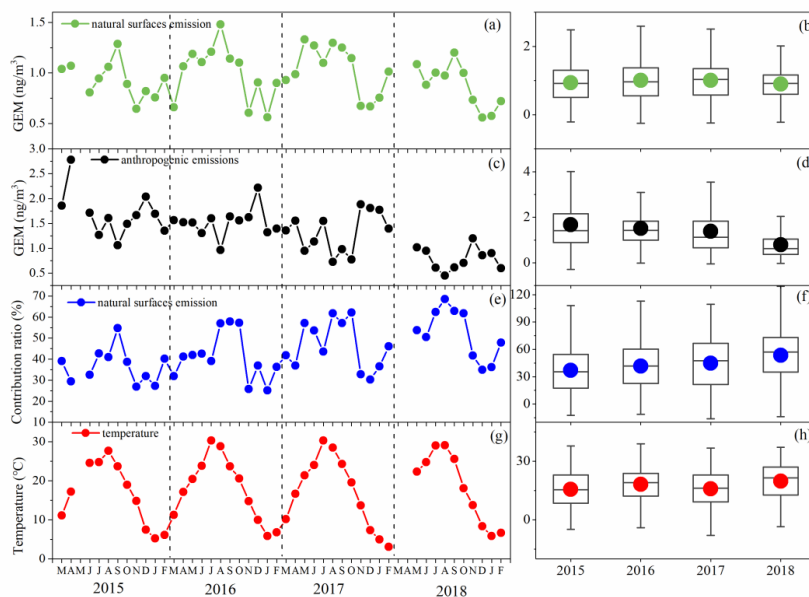
547

548

549   Figure 5. Contributions of natural surface emissions and anthropogenic sources to atmospheric

550   GEM in the four seasons during 2015 – 2018.

551

552

Figure 6. The monthly and annual GEM concentrations contributed by natural surface emissions (a-b) and anthropogenic emissions (c-d) from 2015 to 2018. (e-f) The monthly and annual contribution of natural surface emissions to GEM concentrations from 2015 to 2018. (g-h) The corresponding ambient temperature from 2015 to 2018.